Quaternary Science Reviews 137 (2016) 113–125

Contents lists available at ScienceDirect

Quaternary Science Reviews

journal homepage: www.elsevier.com/locate/quascirev

Multiple water isotope proxy reconstruction of extremely low last glacial temperatures in Eastern Beringia (Western Arctic)

Trevor J. Porter [a, b, *], Duane G. Froese [b], Sarah J. Feakins [c], Ilya N. Bindeman [d], Matthew E. Mahony [b], Brent G. Pautler [e, i], Gert-Jan Reichart [f, g], Paul T. Sanborn [h], Myrna J. Simpson [i, j], Johan W.H. Weijers [f, 1]

[a] Department of Geography, University of Toronto Mississauga, Mississauga, ON, L5L 1C6, Canada
[b] Earth and Atmospheric Sciences, University of Alberta, Edmonton, AB, T6G 2E3, Canada
[c] Department of Earth Sciences, University of Southern California, Los Angeles, CA, 90089, USA
[d] Department of Geological Sciences, University of Oregon, Eugene, OR, 97403, USA
[e] Advanced Chemistry Development, Inc., Toronto, ON, M5C 1B5, Canada
[f] Department of Earth Sciences, Utrecht University, P.O. Box 80.021, 3508 TA, Utrecht, The Netherlands
[g] Royal Netherlands Institute for Sea Research, Department of Ocean Systems, P.O. Box 59, 1790 AB, Den Burg, Texel, The Netherlands
[h] Ecosystem Science and Management Program, University of Northern British Columbia, Prince George, BC, V2N 4Z9, Canada
[i] Department of Physical & Environmental Sciences, University of Toronto Scarborough, Toronto, ON, M1C 1A4, Canada
[j] Environmental NMR Centre, University of Toronto Scarborough, Toronto, ON, M1C 1A4, Canada

ARTICLE INFO

Article history:
Received 4 October 2015
Received in revised form
6 February 2016
Accepted 9 February 2016
Available online 17 February 2016

Keywords:
Eastern Beringia
Precipitation isotopes
Temperature reconstruction
Relict ice
Hydrated volcanic glass shards
Fossil plant waxes

ABSTRACT

Precipitation isotopes are commonly used for paleothermometry in high latitude regions. Here we present multiple water isotope proxies from the same sedimentary context – perennially frozen loess deposits in the Klondike Goldfields in central Yukon, Canada, representing parts of Marine Isotope Stages (MIS) 4, 3 and 2 – allowing us to uniquely corroborate fractionations and temperature conversions during these Late Pleistocene cold stages. We include new and existing proxy data from: relict wedge ice, a direct archive for snowmelt; relict pore ice, an archive for bulk soil water integrating year-round precipitation; and hydrated volcanic glass shards and fossil plant waxes, which are also thought to integrate year-round precipitation but are subject to large fractionations. In some cases, our temperature estimates based on existing proxy data are much cooler than previously estimated due to our use of source water corrections for the glacial ocean, new transfer functions calibrated specifically for northern North America ($\delta D_{precip} = 3.1‰ \cdot {}^{\circ}C^{-1} \times T - 155‰$; and $\delta^{18}O_{precip} = 0.41‰ \cdot {}^{\circ}C^{-1} \times T - 20.2‰$), and novel insights on the apparent net fractionation correction for Eastern Beringian steppe-tundra plant waxes ($\varepsilon_{wax/precip} = -59 \pm 10‰$). The snowmelt origin of wedge ice ensures a relatively constrained winter-spring seasonality of contributing precipitation, as supported by the consistency between water isotope measurements from Late Holocene wedge ice and modern winter-spring precipitation. Wedge ice dating to the transitional MIS 3/2 is isotopically depleted relative to modern spring-winter precipitation by an amount that indicates a temperature depression of ~14 ± 5 °C below modern. The soil water origin of pore ice, and other proxies integrating year-round precipitation from soil water, allows for a more variable precipitation seasonality. The isotopic composition of modern pore ice is consistent with mean annual precipitation. However, the isotopic composition of pore ice during MIS 3/2 converges on wedge ice values, signalling an increase in the ratio of cold-to-warm-season precipitation integrated by pore ice during glacial times, possibly due to drier summers as supported by the fossil record and climate model simulations. In the study region, water isotope proxies integrating year-round precipitation may overestimate annual temperature differences between today and recent cold stages due to transient precipitation seasonality, as detected here, and thus are best interpreted as upper bound estimates. Based on these proxies, we estimate that annual temperatures during MIS 4, 3/2 and 2 were depressed below the modern climate to a maximum of ~18 °C, 16 °C and 21 °C ± 4–5 °C, respectively. Our study highlights the

* Corresponding author. Department of Geography, University of Toronto Mississauga, Mississauga, ON L5L 1C6 Canada.
E-mail address: trevor.porter@utoronto.ca (T.J. Porter).
[1] Present address: Shell Global Solutions International, 2288 GS, Rijswijk, The Netherlands.

http://dx.doi.org/10.1016/j.quascirev.2016.02.006

value of multiple water isotope proxies towards understanding changes in precipitation seasonality and developing robust reconstructions of past climate, and may be particularly important for studies of the major climate transformations over glacial-interglacial timescales.

1. Introduction

In the Northern Hemisphere, water isotopes from ice cores provide detailed records of paleotemperature since the last interglacial (Johnsen et al., 2001), but are not well distributed spatially. In continental regions, diverse proxy-based evidence from lake sediments, paleosols and tree-rings is used to fill spatial gaps in the paleoclimate field, but many such archives in northern North America document only the post-glacial period due to glacial scouring of the land-surface. Perennially-frozen loess deposits, known as 'mucks' or 'Yedoma' in unglaciated Yukon and Alaska (Schirrmeister et al., 2013), overcome this temporal limitation and provide a rare opportunity to reconstruct Late Pleistocene climates in continental North America (Froese et al., 2009). Mucks offer a rich archive for precipitation isotopes in relict ice (Froese et al., 2006), and other proxies such as hydrated tephra (Friedman et al., 1993a) and plant waxes (Sachse et al., 2012) which record precipitation isotopes, but modified by fractionations associated with the relevant reactions. The depositional age of mucks can be determined by tephrochronology (Preece et al., 2011) and radiocarbon dating of fossils preserved in the frozen sediments (Fraser and Burn, 1997; Zazula et al., 2006), and thus provide a well-dated record of paleoenvironmental change while overcoming some of the spatiotemporal limitations associated with other high latitude proxy archives.

Kotler and Burn (2000) were first to estimate the magnitude of deglacial warming in the Klondike Goldfields region (Fig. 1) based on stable oxygen isotope ratios ($\delta^{18}O$) of relict ice in mucks, a $\delta^{18}O_{precip}$ proxy. Kotler and Burn (2000) estimated full glacial paleotemperatures to be ~11 °C cooler than today assuming Dansgaard's (1964) temperature-$\delta^{18}O_{precip}$ line (Equation (1)). A more recent study by Pautler et al. (2014) examined the stable hydrogen isotope ratios of plant *n*-C_{29} alkanes (δD_{wax}), a δD_{precip} proxy, in Klondike mucks dating to the penultimate cold stage, Marine Isotope Stage (MIS) 4, and transitional MIS 3/2. Based on biomolecular data from the mucks (Pautler et al., 2013), Pautler et al. (2014) approximated the contributing paleoflora to be primarily graminoid, which has an apparent net fractionation ($\varepsilon_{wax/precip}$) of −149‰ (Sachse et al., 2012), and used Equation (2) to solve for δD_{precip} based on the δD_{wax} measurements. Pautler et al. (2014) applied an 8‰ source water correction to account for the enriched glacial ocean, and used Dansgaard's (1964) temperature-δD_{precip} line (Equation (3)) to estimate that Mean Annual Temperatures (MATs) were ~6 °C colder than modern during MIS 4 and 3/2.

$$\delta^{18}O_{precip} = 0.69_5‰\cdot{}^{\circ}C^{-1} \times \text{temperature}(^{\circ}C) - 13.6‰ \text{ (Dansgaard, 1964)} \quad (1)$$

$$\varepsilon_{wax/precip} = 1000 \times \left[(\delta D_{wax} + 1000)/(\delta D_{precip} + 1000) - 1\right] \text{ (Sachse et al., 2012)} \quad (2)$$

$$\delta D_{precip} = 5.6‰\cdot{}^{\circ}C^{-1} \times \text{temperature } (^{\circ}C) - 100‰ \text{ (Dansgaard, 1964)} \quad (3)$$

We propose revised paleotemperatures based on the datasets of Kotler and Burn (2000) and Pautler et al. (2014) to account for several factors that significantly influence the results: (1) ocean source water enrichment; (2) region-specific temperature-water isotope systematics; and (3), of relevance to Pautler et al. (2014) only, novel insights on the $\varepsilon_{wax/precip}$ for the steppe-tundra paleoflora. We revisit these Klondike mucks to explore a powerful combination of direct and proxy-based evidence for precipitation isotopes during MIS 4, 3/2 and 2, including new and existing data from relict wedge ice, pore ice, hydrated volcanic glass shards, and fossil plant waxes. We offer revised paleotemperature estimates based on new temperature-δD_{precip} and temperature-$\delta^{18}O_{precip}$ regression lines calibrated specifically for northern North America. Fossil plant waxes (Sachse et al., 2012) and hydrated volcanic glass shards (Friedman et al., 1993a) in the geologic record provide indirect estimates of δD_{precip}, but various fractionations that are not always well known must be assumed and can be a large source of uncertainty. Relict ice offers a direct measurement of δD_{precip} (Meyer et al., 2015) and, thus, comparison with δD proxies from the same deposits provides an opportunity to constrain the net fractionations of δD proxies. We take advantage of this unique situation to constrain the $\varepsilon_{wax/precip}$ of the contributing steppe-tundra paleoflora, and validate the empirical fractionation line proposed by Friedman et al. (1993a) to estimate δD_{precip} from the δD of hydrated volcanic glass shards.

2. Background

2.1. Temperature-water isotope relations

Paleotemperatures can be estimated from proxy estimates of δD_{precip} (or $\delta^{18}O_{precip}$) given an appropriate transfer function. At mid- to high latitudes, the relation between air temperature and precipitation isotopes is strong, as demonstrated by the empirical regression lines developed by Dansgaard (1964) for the relations between MAT and $\delta^{18}O_{precip}$, and MAT and δD_{precip}, based on data from North Atlantic island sites, and Greenland and Antarctica ice caps (Equations (1) and (3)). Similar lines have been applied to ice core records from Greenland and Antarctica to estimate temperatures spanning the glacial-interglacial climate transition (Johnsen et al., 2001), however changes in precipitation seasonality can affect the accuracy of such reconstructions (Edwards et al., 1996; Johnsen et al., 2001). Furthermore, the precipitation temperature-isotope relation is not spatially uniform, but can vary due to differences in moisture source, continentality and rainout history, which are related to atmospheric circulation and topography (Birks and Edwards, 2009; Rozanski et al., 1993). Thus, regionally appropriate transfer functions must be considered.

2.2. d-excess of precipitation and relict ice

The Global Meteoric Water Line (GMWL; $\delta D = 8 \times \delta^{18}O + 10‰$; Craig, 1961) describes the general relation between δD and $\delta^{18}O$ in mean annual global precipitation. The GMWL slope of 8 reflects the progressive rainout of heavy water isotopes as moist air condenses during ascent or poleward transport, approximating Rayleigh

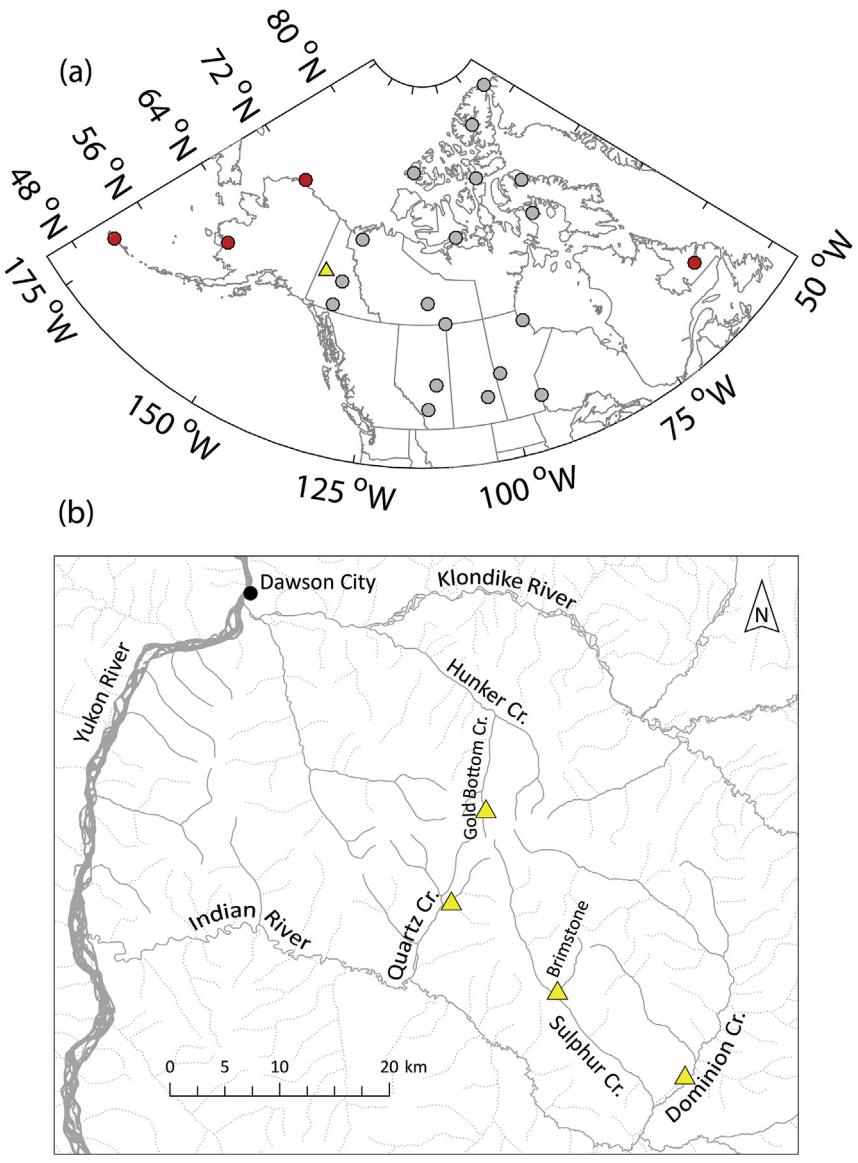

Fig. 1. (a) Map showing the location of the Klondike Goldfields area and GNIP stations of interest - continental (grey circles) and maritime-influenced (red circles). (b) Map of study sites (triangles) in the Klondike Goldfields. (For interpretation of the references to colour in this figure legend, the reader is referred to the web version of this article.)

distillation. The deuterium-excess (d-excess $= \delta D - 8 \times \delta^{18}O$) of +10‰ for average global precipitation reflects non-equilibrium (fast) fractionation of the initial vapour at the moisture source, and relates to the lower diffusivity of $H_2^{18}O$ relative to HDO in the vapour phase. However, d-excess of most precipitation deviates from +10‰ due to the combined kinetic effects of several other factors, including sea surface temperature and the ocean-atmosphere evaporative gradient at the moisture source, continental moisture recycling from evapotranspiration, kinetic effects specific to solid-phase precipitation, and evaporation of rain below the cloud (Aemisegger et al., 2014; Gat et al., 1994; 2003; Jouzel and Merlivat, 1984; Merlivat and Jouzel, 1979; Pfahl and Sodemann, 2014). For systems where continental moisture recycling is negligible, topography is relatively simple and precipitation inputs are mostly of one phase (e.g., snow), d-excess may be a reliable proxy for variability in evaporative conditions at a constant moisture source, or shifting source regions due to an alternative atmospheric circulation. Over glacial-interglacial timescales, such interpretations have been made based on the Greenland and Antarctica ice core records (Jouzel, 2013; Jouzel et al., 2007). More locally, the Barrow Ice Wedge System, Alaskan north coast, documents pronounced d-excess trends during the Younger Dryas interval that is consistent with the Greenland NGRIP record, and has been interpreted as a large-scale atmospheric reorganisation that impacted the pan-Arctic (Meyer et al., 2010).

2.3. Precipitation in relict ice

Relict permafrost is an archive for ancient precipitation isotopes and climate change, including ice cores from polar ice caps (Jouzel, 2013). In sedimentary contexts, precipitation isotopes are archived in relict wedge and pore ice (Fritz et al., 2012; Kotler and Burn, 2000; Lacelle et al., 2007; Schwamborn et al., 2006; Wetterich et al., 2011), although these archives have not been widely used in Quaternary paleoclimate studies.

Ice wedges form by thermal contraction cracking of the ground during the cold season, extending from the surface to below the permafrost table, followed by snowmelt infilling during springtime and re-freezing at negative ground temperatures (Lachenbruch, 1962). The ice wedge itself can crack during subsequent winters

and grow by the same sequence of events. Multi-year ice wedges contain multiple ice veins, each representing a growth event, and may remain active for centuries under suitable conditions (Meyer et al., 2010). Thermal contraction cracking is often associated with rapid cooling sustained over several days, especially where snow depths are small and do not significantly limit thermal diffusion (Mackay, 1993). Because wedge ice is a product of winter-spring precipitation, the δD or $\delta^{18}O$ of wedge ice provides an opportunity to reconstruct cold-season paleotemperatures (Meyer et al., 2010; 2015).

Relict pore ice represents soil water, derived from snowmelt and summer precipitation, that percolated to maximum thaw depths and became entombed in permafrost (Kotler and Burn, 2000; Mackay, 1983). Pore ice or interstitial ice is frozen *in situ* in the active layer (French and Shur, 2010). It may undergo numerous freeze-thaw cycles, each time potentially integrating new precipitation and pore ice from greater thaw depths, and eventually may integrate several years of precipitation (Schwamborn et al., 2006). Aggradation of the surface by organic and inorganic sedimentation causes an upward adjustment of the permafrost table. Pore ice that is overtaken by the permafrost table will remain frozen barring an exceptionally deep thermal erosion event (e.g., fire or an unusually warm summer). Accumulation of Klondike mucks during Pleistocene cold stages was paced by rapid loess deposition under cold, dry conditions, and provides a frozen record of precipitation isotopes and paleoenvironmental change (Fraser and Burn, 1997; Froese et al., 2009).

2.4. Hydrated volcanic glass shards

Volcanic glass shards, a primary fraction of volcanic ash or tephra, are formed by the rapid cooling of ejected magma during an eruption. Newly formed rhyolitic glass shards initially contain low H_2O concentrations, ~0.1–0.3% by weight (Friedman and Smith, 1958; Friedman et al., 1993a). Following the eruption and deposition in sedimentary contexts, environmental waters (or 'secondary hydration waters') diffuse irreversibly into the glass shards over several millennia until they are saturated to ~3.5% H_2O by weight (Ross and Smith, 1955). The δD of the glass shards and the secondary hydration waters are offset in value due to a fractionation associated with the diffusion process. This fractionation has been constrained by Friedman et al. (1993a), Equation (4), and can be used to estimate δD_{precip} from the δD of hydrated glass shards. In the Klondike, deep groundwater flow is precluded due to permafrost, and thus waters in contact with bedded tephras will derive mostly from precipitation contributing to soil water. Regionally distributed tephras such as the Dawson tephra, radiocarbon dated to 25.3 ^{14}C ka BP (*ca.* 29.4 cal ka BP) (Zazula et al., 2006), are well-preserved in muck deposits in the Klondike Goldfields but have not yet been used to estimate δD_{precip} in this region.

$$\delta D_{\text{environmental water}} = 1.0343 \times \left(1000 + \delta D_{\text{glass}}\right) - 1000 \text{ (Friedman et al., 1993a)} \quad (4)$$

2.5. Fossil plant waxes

The waxy coating of plants includes both *n*-alkanes and *n*-alkanoic acids (Eglinton and Hamilton, 1967), which are widely used terrestrial vegetation biomarkers in paleoenvironmental studies (Feakins et al., 2012; Pagani et al., 2006; Tierney et al., 2008). The δD of plant wax is a commonly used proxy for δD_{precip}, but is offset in value due to the combined effects of several kinetic and biochemical fractionations (Sachse et al., 2012), referred to as the 'apparent or net fractionation' ($\varepsilon_{wax/precip}$), see Equation (2). Large $\varepsilon_{wax/precip}$ variations exist between plant types, species and across climate and latitudinal gradients (Sachse et al., 2012; Yang et al., 2011), and thus uncertainty in the value of $\varepsilon_{wax/precip}$ can be one of the largest uncertainties in reconstructing δD_{precip} and climate based on δD_{wax}.

3. Methods

3.1. GNIP water isotope data

The Global Network for Isotopes in Precipitation (GNIP) dataset (IAEA/WMO, 2014) was used to characterise relations between air temperature and precipitation isotopes (δD, $\delta^{18}O$) by linear regression for mid- to high-latitude (>50°N) North American sites. Only stations with monthly records were included in the analysis. Twenty-two stations satisfied these criteria (Fig. 1a). The co-isotopic behaviour of this local precipitation data was also evaluated with respect to the GMWL, and this framework was used as a basic test of conformity to determine if Klondike relict ice is similar to modern precipitation and, therefore, if it is reasonable to interpret ancient waters in the context of modern climate-isotope systematics.

3.2. Permafrost samples – relict ice, tephra and plant waxes

Relict ice was collected from two muck exposures in the Klondike Goldfields – Quartz Creek and Brimstone (Fig. 1b). Quartz Creek is a well-known locality hosting perennially frozen massively bedded loess and steppe-tundra macrofossils of MIS 4 and 3/2 age (Fraser and Burn, 1997; Zazula et al., 2011). Brimstone on Sulfur Creek is a newly exposed site hosting perennially frozen, organic-rich sediments with abundant woody macrofossils of Holocene age. Ice samples were collected by axe or gas-powered drill with a diamond-tipped coring barrel (3 inch diameter and 24 inch length), stored in field freezers, and shipped frozen to the University of Alberta. The ice samples were thawed at 4 °C and the supernatant was filtered into 2 ml vials for water isotope analysis using a Picarro L2130-*i* analyser (1σ precision was 0.5‰ for δD and 0.1‰ for $\delta^{18}O$ for an in-house water standard). Reference standards USGS 45 (δD = −10.3‰, $\delta^{18}O$ = −2.24‰) and USGS 46 (δD = −235.8‰, $\delta^{18}O$ = −29.80‰) distributed by the U.S. Geological Survey at Reston, Virginia, were used to normalize results to the Vienna Standard Mean Ocean Water (VSMOW)-Standard Light Antarctic Precipitation (SLAP) isotopic scale. Plant macrofossils associated with relict ice samples were AMS ^{14}C dated at the University of California Irvine.

A sample of Dawson tephra collected by Froese et al. (2006) at Goldbottom Creek (Fig. 1b) was prepared for δD analysis. The sample was wet sieved (200–325 mesh, or 44–74 μm) to isolate a consistent size fraction and rinse away adhesive clays. Lithium Sodium Polytungstate was used to separate glass shards from accessory minerals by density. The glass separate was inspected under polarized light to ensure the absence of minerals. The sample was dried in an evaporator oven, and its δD was measured on a TC/EA-MAT-253 continuous flow system at the University of Oregon following Nolan and Bindeman (2013) protocols (1σ precision was 1‰–2.6‰ for mica standards).

One of the muck samples from Quartz Creek was also analysed for the δD_{wax} of long-chain *n*-alkanoic acids. This sample offers a comparison with Pautler et al.'s (2014) *n*-C_{29} δD_{wax} data to test δD differences between two compound classes (*n*-alkanes and *n*-alkanoic acids) for the MIS 3/2 time slice. The sample was freeze-dried and homogenized. Seven sub-samples were processed. The soluble lipids were extracted using a Dionex Accelerated Solvent Extractor 300 and 9:1 DCM:methanol. The *n*-alkanoic acids were

isolated by standard Si-gel chromatography methods, as described elsewhere (Tierney et al., 2008). The *n*-alkanoic acids were methylated to Fatty Acid Methyl Esters (FAMEs) and analysed by GC-IRMS (Agilent GC-Thermo Finnigan Delta V; 1σ precision = 2‰) at the G.G. Hatch Stable Isotope Laboratory, University of Ottawa. The A5 mix reference standard distributed by Arndt Schimmelmann, Indiana University, was used to calibrate the raw δD values to the VSMOW-SLAP scale. Calibrated FAME δD values were stoichiometrically corrected to account for the three hydrogen atoms contributed during the methylation step (methanol δD = −143.4‰) to yield corrected n-alkanoic acid δD_{wax} values (see Supporting Information for calculations).

4. Results and discussion

4.1. The temperature-water isotope line for sub-Arctic/Arctic North America

The temperature-δD_{precip} relation of 22 North American sites that satisfied the selection criteria was examined (Fig. 1a). Four of these sites (Adak, Anchorage, Barrow and Goose Bay) have a temperature-δD_{precip} response that is inconsistent with the other 18 sites (Fig. 2). We refer to these 4 sites as 'maritime' influenced because they coincide roughly with maritime Polar (mP) air mass regions. The other 18 sites are termed 'continental' as they coincide with source regions of continental Polar (cP) and continental Arctic (cA) air masses, which are drier and more stable than mP air (Bryson, 1966; Wendland and Bryson, 1981). For the northern latitudes, continental air is fundamentally different from maritime air because it is isolated from its evaporative origin and unable to re-exchange with ocean water. The relatively immature rainout history of maritime air may explain why maritime precipitation it is enriched compared to continental precipitation at any given temperature (Rozanski et al., 1993). For this study, we focus on the continental GNIP stations which are most relevant for interpreting water isotope proxies in continental Yukon. The temperature-δD_{precip} line for these sites is given in Equation (5), and the temperature-$\delta^{18}O_{precip}$ line is given in Equation (6), where 'T' is near surface air temperature in degrees Celsius.

$$\delta D_{precip} = (3.1\pm0.1)‰^{\circ}C^{-1} \times T - (155\pm1)‰;\ 1\sigma_{residuals} = \pm 28‰;\ r = 0.87 \quad (5)$$

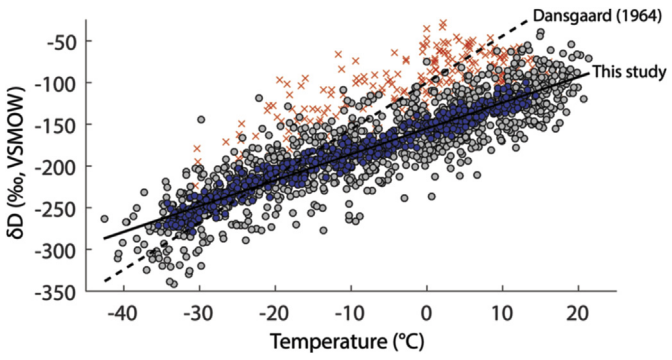

Fig. 2. A comparison of raw monthly δD_{precip} and air temperatures for maritime-influenced sites (red 'x') and continental sub-Arctic and Arctic sites (grey circles). A regression line (solid line; $\delta D_{precip} = 3.1‰\cdot^{\circ}C^{-1} \times T - 155‰$) is provided for the continental sub-Arctic/Arctic data. The Dansgaard (1964) temperature-δD_{precip} regression line is plotted for comparison (dashed line). Twelve-month averages (blue circles) for the continental sub-Arctic and Arctic sites are plotted to demonstrate the attenuation of sampling error at timescales greater a one month. (For interpretation of the references to colour in this figure legend, the reader is referred to the web version of this article.)

$$\delta^{18}O_{precip} = (0.41\pm0.01)‰^{\circ}C^{-1} \times T - (20.2\pm0.1)‰;\ 1\sigma_{residuals} = \pm 3.70;\ r = 0.87 \quad (6)$$

The slope of the North American temperature-δD_{precip} line is roughly half as steep as the slope of the Dansgaard (1964) calibration (5.6‰·°C^{-1}; Fig. 2), demonstrating the importance of regionally appropriate calibrations (Rozanski et al., 1993). However, similar temperature-isotope coefficients are also observed in northeastern Siberia (Wilkie et al., 2013). There is substantial noise in the North American regression when monthly GNIP data are plotted (Fig. 2). Monthly residuals have a 28‰ standard deviation, and a Gaussian distribution (Supporting Information) implying a random process. Variability in moisture source or atmospheric circulation may be a factor (Birks and Edwards, 2009). However, sampling error inherent to monthly GNIP records is likely a greater source of uncertainty. Monthly GNIP records consist of measurements of δD and $\delta^{18}O$ from a monthly precipitation sample, paired with local air temperatures averaged monthly. The monthly precipitation sample is a composite of all precipitation that fell during the sampling interval, collected in a single reservoir, resulting in a blended sample that is isotopically weighted by the contributions of each precipitation event (IAEA/WMO, 2014). The theoretical relation between air temperature and precipitation isotope composition can be approximated by a first-order polynomial function (e.g., Eq. (5)). However, this relation may be obscured by large residuals when monthly precipitation isotope data are plotted against monthly air temperatures, since monthly air temperature may differ greatly from the mean air temperature of days that contributed to the precipitation sample. In extreme cases when a 'monthly' precipitation sample derives from a single precipitation event on a single day, plotting monthly temperature versus monthly δD_{precip} may be expected to manifest as a large residual. Conversely, small residuals are expected if precipitation is evenly distributed across the monthly sampling interval in timing and amount, in which case monthly temperature is more likely to represent the period integrated by the precipitation sample.

Because this type of error is random and normally distributed, it can be attenuated by averaging, as is evident in Dansgaard's (1964) temperature-isotope regression based on mean annual values from the ice caps and North Atlantic sector. The same attenuation of error can be simulated for the North American stations by calculating 12-month averages from monthly data (see Supporting Information). The spread of residuals for the 12-month averages is greatly improved compared to the raw monthly data (Fig. 2; correlation improves from r = 0.87 to 0.98). When Equation (5) is solved for temperature, this attenuation of error can be quantified using the standard error of the estimate (σ_{SEE}). For the raw monthly data σ_{SEE} is ±9.1 °C, but reduces to ±2.9 °C for 12-month averages. The 12-month σ_{SEE} likely reflects uncertainties that are unrelated to sampling error (e.g., variability in source region and atmospheric circulation), some of which might be further attenuated over geologic timescales. We adopt an σ_{SEE} of ±2.9 °C for our paleotemperature estimates based on δD_{precip} proxies, but with the caveat that this may still be conservative when applied to proxies that integrate δD_{precip} over long timescales. The same σ_{SEE} is justified for $\delta^{18}O_{precip}$-based temperature estimates.

Paleotemperatures can be estimated based on Equation (5) and proxy-δD_{precip}, but a source-water correction must be made for the glacial ocean, which was enriched in heavy isotopologues due to light water storage in ice sheets. Pore waters in marine sediments from the Last Glacial Maximum (LGM) show that sea water $\delta^{18}O$ and δD ($\delta^{18}O_{sw}$ and δD_{sw}) were +0.7–1.1‰ and +6–9‰,

respectively, compared to today (Malone et al., 2004; Schrag et al., 2002). Global ice sheets during MIS 4 and 3/2 were less extensive compared to the LGM, and it follows that $\delta^{18}O_{sw}$ and δD_{sw} during MIS 4 and 3/2 were probably less positive than LGM values. Rohling et al. (2014) estimated $\delta^{18}O_{sw}$ for the last 5.3 Ma based on a deconvolution of their sea level reconstruction and a global stack of foraminifera $\delta^{18}O$ records by Lisiecki and Raymo (2005). Rohling et al.'s (2014) $\delta^{18}O_{sw}$ estimates for MIS 4 and 3/2 are ~ +0.6‰ relative to today, or roughly two-thirds of the offset between the LGM and modern sea water. We assume the δD_{sw} offset during MIS 4 and 3/2 was proportional to the $\delta^{18}O_{sw}$ offset, or ~ +5‰ relative to modern.

Finally, it is important to note that modern temperature-isotope relations are not always appropriate for Late Pleistocene relict ice. For example, in central Greenland, the modern temperature-isotope slope underestimates the true magnitude of deglacial warming by a factor of 2 based on deep ice core records, owing to precipitation seasonality differences (Johnsen et al., 2001). However, modern slopes appear to provide a reasonable first-order approximation of deglacial warming in Antarctica based on the Vostok and EPICA Dome C ice cores (Jouzel et al., 2003). The potential for an altered slope in continental North America is unknown. However, isotope-enabled GCMs have provided useful insights on temperature-isotope relation stability elsewhere under changing boundary conditions (LeGrande and Schmidt, 2009; Werner and Heimann, 2002), and similarly could be used to evaluate such changes in Eastern Beringia.

4.2. Co-isotopes in precipitation and relict ice

In co-isotope (δD-$\delta^{18}O$) space, the North American continental GNIP data are in close general agreement with the GMWL over a large δ_{precip} range (Fig. 3a), indicating that continental precipitation is governed by the same fractionations as most extra-tropical precipitation. The Local Meteoric Water Line (LMWL) that best fits the North American dataset has a slope of 7.6, compared to 8 for the GMWL, which is consistent with other sites in the eastern Arctic (Edwards et al., 2004). We also find that δ_{precip} for the Yukon GNIP stations, Whitehorse and Mayo, which are proximal to the Klondike study region, is in general agreement with the GMWL and covers a wide δ_{precip} range, ~220‰ and ~20‰ for δD and $\delta^{18}O$, respectively. Notably, this range overlaps almost entirely with the Klondike relict ice samples that we evaluate as climate proxies in greater detail below.

Beyond the general co-isotopic trend of these data, there is significant variability around the GMWL, which is best expressed in terms of *d*-excess. The typical (5–95 percentile) range of *d*-excess for the continental dataset is from ~ −10‰ to +20‰ depending on month (Fig. 3b). Because *d*-excess is sensitive to moisture source, and considering the large geographic coverage of the continental GNIP dataset which likely integrates precipitation inputs from many source regions, it is appropriate to focus our analysis on the two Yukon stations which are primarily fed by the North Pacific year-round (Lackman and Gyakum, 1996; Petrone and Rouse, 2000; Szeto et al., 2008), which are the best analogues for interpreting *d*-excess in Klondike relict ice. In spite of being primarily Pacific-sourced, the Yukon sites are characterised by large monthly *d*-excess ranges that are consistent with the other continental sites, and for some months they define the extreme ranges (e.g., February, −27 to +28‰; and March, −40 to +32‰). Overall, these results imply that continental *d*-excess is inherently highly variable at monthly timescales, and likely owes to factors other than just moisture source.

The Yukon GNIP records and the larger continental dataset also exhibit a small seasonal trend in *d*-excess (~5‰ amplitude; Fig. 3).

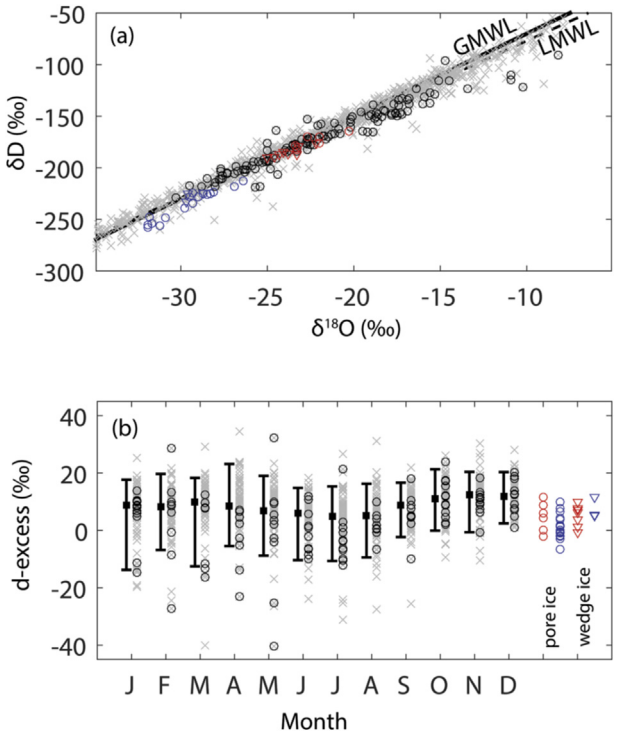

Fig. 3. (a) Monthly δD and $\delta^{18}O$ for the continental GNIP records (grey 'x'), plotted on the Global Meteoric Water Line (GMWL) and the Local Meteoric Water Line (LMWL; m = 7.6). Data for the two local Yukon GNIP stations, Mayo and Whitehorse, are indicated (black open circles). Relict ice – Holocene pore/wedge ice (red circles/red triangles) and Late Pleistocene pore/wedge ice (blue circles/blue triangles); all relict ice data in Supporting Information. (b) *d*-excess by month for the same GNIP and relict ice data; 5–95% range and median values are indicated for the GNIP data. (For interpretation of the references to colour in this figure legend, the reader is referred to the web version of this article.)

The higher *d*-excess of cold-season precipitation is linked to the kinetic fractionation specific to snow formation, and lower values to below-cloud evaporation of falling rain (Edwards et al., 2004). The seasonal trend is well defined by the large continental dataset. The Yukon dataset is more limited in number of observations, but generally has similar mean *d*-excess values during the cold-season months, and slightly lower mean values in mid-summer. The typical range of *d*-excess in modern Yukon precipitation is reflected in the Klondike pore ice and wedge ice, but with a notable difference that the relict ice does not appear to record extreme values. This result is expected because relict ice integrates several months of precipitation, which would dampen variability in the blended mean. There is still some *d*-excess variability in relict ice (wedge ice, 0 to +11‰; pore ice, −7 to +11‰), which can be explained by weather fluctuations in precipitation timing, amount and type (snow vs. rain), and integration of the occasional extreme value. Overall, we find a slightly higher mean *d*-excess for the wedge ice compared to pore ice (+6‰ vs. +2‰, respectively), which is explained by the snowmelt-origin of wedge ice and the seasonally higher *d*-excess of cold-season precipitation. Conversely, pore ice is less constrained to a winter-spring season of formation (the active layer must be thawed for it to be incorporated) and thus may reflect average soil waters which represent precipitation inputs from all seasons.

The Greenland GRIP and NGRIP ice cores (Jouzel et al., 2007) and Barrow ice wedges (Meyer et al., 2010) document clear 'source region' signals in *d*-excess across the major stadial-interstadial and Dansgaard-Oeschger transitions, with maximum amplitudes that

generally do not exceed 5‰. As discussed, we find much larger *d*-excess amplitudes in the Klondike relict ice, which can be more simply attributed to the large number of kinetic effects acting on continental precipitation. Comparatively, the Greenland ice cores and Barrow ice wedges may avoid some of these confounding effects by sampling mainly one type of precipitation (i.e., snow), and because the contribution of recycled continental moisture to those systems is negligible.

Based on the available co-isotope data, we find no major differences between past and present meteoric waters in the Klondike. We interpret this as evidence that paleometeoric waters in continental Yukon can be interpreted in the framework of modern climate-isotope systematics.

4.3. Wedge ice

Wedge ice offers the prospect of cold-season paleotemperature estimates since the isotopic composition of wedge ice derives from cold-season precipitation, which is associated with cold-season temperatures. At Brimstone, three ice samples were collected across a ~30 cm wide ice wedge of Late Holocene age (*ca.* 0–500 years BP; Supporting Information). The δD mean of the Brimstone wedge is −187 ± 3‰ ($1\sigma_{stdev}$; Table 1). This value is similar to a δD mean of −184 ± 6‰ calculated from five Holocene ice wedges (precise ages, sites not specified) from Kotler and Burn (2000). The Brimstone δD mean also agrees with the Oct-May δD_{precip} mean of −191‰ for precipitation at the local GNIP station at Mayo (~180 km east; full period of record is 1986–1988), corresponding to the season of snow accumulation and first melt. This agreement supports the notion that wedge ice δD reflects cold-season precipitation (Meyer et al., 2015). We also find good agreement between Oct-May near-surface air temperatures for the Klondike area (−12.2 °C; Kalnay et al., 1996) and 'inferred' temperatures calculated based on the Brimstone ice wedge δD mean and Equation (5) (~ −10 ± 3 °C, 1c.σ − compounded standard deviation; refer to Supporting Information for details on calculated values). This agreement indicates that Equation (5) is well-calibrated for paleotemperature estimates from relict ice in this region.

Single cores were collected from the centre of three narrow (~10–15 cm) ice wedges at Quartz Creek with MIS 3/2 ages spanning 31.9–30.2 cal ka BP (Supporting Information). The δD mean of these ice wedges is −227 ± 5‰ (Table 1). This value is depleted by ~45‰ relative to the Brimstone wedge ice δD mean after correcting for a δD_{sw} offset of 5‰, indicating colder temperatures. The isotopic difference suggests that cold-season temperatures during MIS 3/2 were depressed by 14.5 ± 3.3 °C (1 c.σ) below modern (Table 2); the c.σ reflects the Equation (5) σ_{SEE}, and the $1\sigma_{stdev}$ in estimated δD_{precip} for MIS 3/2 and Late Holocene/modern (see Supporting Information for details on calculated values). The reconstruction assumes that the monthly snow budget ratios contributing to the ice wedges were comparable between the two periods. A similar temperature depression of 13.3 ± 3.4 °C (1 c.σ) below modern is calculated using the mean $\delta^{18}O$ from the Brimstone and Quartz Creek ice wedges (Table 2). Minor differences in reconstructed temperature between the two isotopes are expected, in this case ~1.2 °C, due to kinetic effects influencing continental precipitation. Both estimates are valid, and we present their combined mean temperature depression of ~14 ± 5 °C (1c.σ) below modern as the best estimate (Table 3).

These are the first cold-season paleotemperature estimates for this region based on ice wedge water isotopes. Zazula et al. (2006) used fossil insects from Klondike mucks of MIS 3/2 age to estimate the coldest monthly temperature (T_{min}) based on the mutual climate range (MCR) approach and found that T_{min} may have been +0.6 °C to −4.4 °C relative to today. While the fossil beetle proxy has been calibrated to estimate the T_{min} variable, it is known to be a relatively weak predictor of cold-season temperatures in northern regions (Zazula et al., 2011). This is reflected in the large standard error in the mean T_{min} estimate ($1\sigma = \pm 10$ °C), and is thought to reflect the fact that beetles are inactive during the frozen months (Elias, 2001), which is more than half the year in central Yukon. We find it unlikely that similar-to-modern winters would produce precipitation as isotopically depleted as the snowmelt preserved in the Quartz Creek ice wedges.

Table 1
Mean δD and $\delta^{18}O$ values for the target proxies.

Proxy, site	Age BP	δD ± 1σ (‰)	$\delta^{18}O$ ± 1σ (‰)	No. samples
Wedge ice				
[a]Brimstone	*ca.* 0–500 years	$-187_{.4} \pm 2_{.5}$	$-24.4_6 \pm 0.4_5$	3
[b]Unspecified	*ca.* Holocene	$-183_{.7} \pm 5_{.5}$	$-23.4_0 \pm 0.8_9$	5
[a]Quartz Creek	*ca.* 31.9–30.2 cal ka	$-227_{.3} \pm 4_{.5}$	$-29.3_0 \pm 0.5_6$	3
Pore ice				
[a]Brimstone	*ca.* 0–500 years	$-172_{.9} \pm 4_{.9}$	$-22.6_7 \pm 0.6_9$	3
[c]Disturbed forest	post-1950	$-179_{.0} \pm 4_{.2}$	$-22.6_5 \pm 0.9_2$	2
[d]Goldbottom	*ca.* 29.4 cal ka	$-218_{.7} \pm 6_{.0}$	$-27.2_1 \pm 1.0_2$	3
[a]Quartz Creek	*ca.* 31.9–30.2 cal ka	$-226_{.0} \pm 1_{.9}$	$-28.8_5 \pm 0.5_2$	6
[b]Quartz Creek M.	*ca.* 31.2–16.9 cal ka	$-249_{.0} \pm 8_{.4}$	$-31.0_5 \pm 1.0_2$	8
Tephra				
[a]Goldbottom	*ca.* 29.4 cal ka	$-240_{.5} \pm 3_{.3}$	n.a.	3
n-C_{28} acids				
[a]Quartz Creek	*ca.* 31.9–30.2 cal ka	$-268_{.9} \pm 2_{.7}$	n.a.	7
n-C_{29} alkanes				
[e]Quartz Creek	*ca.* 28.0 cal ka	$-264_{.4} \pm 4_{.4}$	n.a.	9
[e]Goldbottom	*ca.* 29.4 cal ka	$-272_{.7} \pm 5_{.5}$	n.a.	4
[e]Quartz Creek	*ca.* MIS 4	$-270_{.1} \pm 8_{.1}$	n.a.	4
[e]Dominion Creek	*ca.* MIS 4	$-275_{.6} \pm 5_{.6}$	n.a.	5

Refer to Supporting Information for details on estimated ages, calculated values and contributing input data. Sub-scripted digits are not significant, but retained here for the propagation of error in subsequent calculations that require these values as inputs.

[a] This study.
[b] Kotler and Burn (2000).
[c] Calmels et al. (2012).
[d] Froese et al. (2006).
[e] Pautler et al. (2014).

Table 2
Reconstructed differences in the precipitation isotope composition (Δδ, source-water corrected) and corresponding paleotemperature depression (ΔT), both relative to modern.

Time slice, proxy	Seasonality	$\delta_{proxy\ mean}$	$\delta_{paleo\ precip}$	$\Delta\delta_{paleo\ -\ modern}$	$\Delta T_{relative\ to\ modern}$
δD proxies					
MIS 3/2, pore ice	annual	$-222._3 \pm 4._8$	$-222._3 \pm 4._8$	−51.4	−16.6 ± 3.6 °C (1 c.σ)
MIS 3/2, wedge ice	cold-season	$-227._3 \pm 4._5$	$-227._3 \pm 4._5$	−44.9	−14.5 ± 3.3 °C (1 c.σ)
MIS 4, n-C_{29} wax	annual	$-272._8 \pm 6._4$	$-226._9 \pm 11._8$	−56.0	−18.1 ± 5.0 °C (1 c.σ)
$\delta^{18}O$ proxies					
MIS 2, pore ice	annual	*n.a.	*n.a.	−8.50	−20.7 ± 4.4 °C (1 c.σ)
MIS 3/2, pore ice	annual	$-28.0_3 \pm 1.0_3$	−28.03 ± 1.0_3	−5.97	−14.6 ± 4.1 °C (1 c.σ)
MIS 3/2, wedge ice	cold-season	$-29.3_0 \pm 0.5_6$	−29.30 ± 0.5_6	−5.44	−13.3 ± 3.4 °C (1 c.σ)

*Δδ for MIS 2 was calculated based on the original ΔT estimate by Kotler and Burn (2000) multiplied by the Dansgaard (1964) temperature-$\delta^{18}O$ coefficient (0.695‰·°C^{-1}); 1 c.σ accounts for 1σ in pore ice $\delta^{18}O$ from Kotler and Burn's (2000) Quartz Creek Member and Organic units, and the σ_{SEE} for Equation (6). Sub-scripted digits are not significant, but retained here for the propagation of error in subsequent calculations that require these values as inputs. Refer to Supporting Information for all calculated values and contributing input data.

Table 3
Summary of mean paleotemperature depressions, averaged by time slice and seasonality.

Time slice	Seasonality	$\Delta T_{relative\ to\ modern}$
MIS 2	annual	−21 ± 4 °C (1 c.σ)
MIS 3/2	annual	−16 ± 5 °C (1 c.σ)
MIS 3/2	cold-season	−14 ± 5 °C (1 c.σ)
MIS 4	annual	−18 ± 5 °C (1 c.σ)

4.4. Pore ice

In the Klondike, pore ice derives from year-round precipitation as we demonstrate below. Importantly for the interpretation of other δD proxies, such as hydrated volcanic glass and fossil plant waxes, pore ice should also represent the same soil waters that are integrated by these other proxies.

The seasonality of precipitation contributing to pore ice is not yet well known. However, if pore ice is a blend of year-round precipitation, the δD of pore ice would be expected to reflect mean annual δD_{precip}. Indeed, we find that the δD mean of Late Holocene pore ice and modern annual precipitation agree closely. Three pore ice samples were collected at Brimstone above and below the ice wedge, roughly coeval in age, with a δD mean of −173 ± 5‰ (Table 1). A similar δD mean of −179 ± 4‰ (Table 1) characterizes young permafrost (including elevated ^3H levels, i.e., post-1950) at a disturbed forest site in the Klondike (Calmels et al., 2012). Kotler and Burn (2000) report a single pore ice δD value of −164‰ from their 'Organic Unit' (*ca.* Holocene) at an unspecified Klondike site, but its precise age is not known. A combined δD mean of −176 ± 5‰ for the Late Holocene/modern samples (this study and Calmels et al., 2012) is consistent with the mean annual δD_{precip} value of −176‰ from the Mayo GNIP station, indicating that recent pore ice reflects annual precipitation and appears to hold some promise as a MAT proxy. For comparison, average winter (Dec-Feb) and summer (Jun-Jul) δD_{precip} values at Mayo are −203‰ and −149‰, respectively. We also find strong agreement between mean annual near-surface air temperatures for the greater Klondike region (−6.1 °C; Kalnay et al., 1996) and inferred air temperatures based on the Late Holocene/modern pore ice δD mean and Equation (5) (~ −7 ± 3 °C; 1c.σ), which again demonstrates that Equation (5) is well-calibrated for paleoclimate estimates in this region.

For the MIS 3/2 time slice, six pore ice samples were collected from Quartz Creek, all bracketed in age by the Quartz Creek ice wedges. The pore ice δD mean is −226 ± 2‰ (Table 1), which is slightly more negative than pore ice reported by Froese et al. (2006) from Goldbottom Creek, associated with the Dawson tephra, with a δD mean of −219 ± 6‰ (Table 1). A combined δD mean including Goldbottom and Quartz Creek pore ice is −222 ± 5‰ (Table 2). Kotler and Burn (2000) report highly depleted pore ice δD values from their Quartz Creek Member ranging from −257‰ to −234‰ (mean = −249 ± 8‰; Table 1), but spanning a wide range of ages from *ca.* 31.2 to 16.9 cal ka BP (precise ages for individual samples are unknown). The most isotopically depleted pore ice reported by Kotler and Burn (2000) likely reflects full glacial conditions and is not directly comparable to our MIS 3/2 pore ice.

Considering the combined δD means for MIS 3/2 pore ice and Late Holocene/modern pore ice, these data imply that mean annual δD_{precip} during MIS 3/2 was depleted by ~51‰ relative to today after correcting by 5‰ for δD_{sw} (Table 2). This ~51‰ δD_{precip} offset implies colder temperatures, and could be interpreted as a MAT depression of 16.6 ± 3.6 °C (1c.σ) below modern (Table 2). A similar MAT depression of 14.6 ± 4.1 °C (1c.σ) below modern is calculated based on pore ice $\delta^{18}O$ from the same deposits (Table 2). The combined MAT depression based on both isotopes is ~16 ± 5 °C (1c.σ) below modern (Table 3). However, this estimate should be interpreted with caution. We note that the δD mean values for the MIS 3/2 pore ice and coeval wedge ice at Quartz Creek are roughly equal (−226‰ vs. −227‰), which implies that the MIS 3/2 pore ice is primarily sampling cold-season precipitation, in contrast to the annual precipitation blend in Late Holocene/modern pore ice.

This result implies a shifting precipitation seasonality between glacial and interglacial times, with a bias in cold stage pore ice towards winter-spring δD_{precip} values. Climate scenarios supporting this result could include an increase in cold-season precipitation and/or a decrease in summer precipitation. The Klondike and Eastern Beringia more broadly was characterised by a steppe-tundra ecosystem with abundant forbs and grasses, and sparse shrub cover (Zazula et al., 2003). This paleoflora draws parallels to both mid-latitude grasslands and forb-rich tundra, and indicates a dry summer scenario. CMIP5/PMIP3 models (Braconnot et al., 2012) constrained by glacial boundary conditions also simulate arid summers in the Klondike. Ensemble means of the four finest resolution CMIP5/PMIP3 models (CCSM4, GISS-E2, MPI-ESM, and MRI-CGCM3; ESGF archive), for best representation of the complex terrain and orographic climate dynamics to the west, indicate summer (Jun-Aug) precipitation totals during the full glacial were less than 35% of the pre-industrial control values, whereas cold-season (Nov-May) precipitation amounts were greater than 70% of the pre-industrial control values. If smaller summer precipitation ratios were sustained throughout the Wisconsinan glacial, this may explain why pore ice δD converges on wedge ice δD during MIS 3/2. In light of the evidence for a shift in precipitation seasonality, the MAT depression of 16 ± 5 °C below modern is best interpreted as a maximum depression.

Kotler and Burn (2000) estimated a full glacial (MIS 2)

temperature depression of ~11 °C below modern based on an observed $\delta^{18}O$ difference of ~ −7.6‰ between Holocene and MIS 2 pore ice. However, this estimate did not account for the $\delta^{18}O_{sw}$ offset and was based on the Dansgaard (1964) temperature-$\delta^{18}O_{precip}$ line, which is ill-suited for this region (Fig. 2). The full glacial temperature depression is re-calculated based on these same data to be ~21 ± 4 °C colder than modern (Tables 2 and 3), assuming a $\delta^{18}O_{sw}$ correction of 0.9‰ for the LGM and Equation (6). This result should also be interpreted as a maximum depression.

The putative precipitation seasonality shift detected from Klondike pore ice, suggesting an increase in the ratio of cold-to-warm season precipitation, draws parallels to Greenland where precipitation seasonality during cold stages may have shifted strongly in the opposite direction toward increased representation of summer precipitation values. Similar to the Klondike, simple interpretation of Greenland ice core records (e.g., Camp Century, NGRIP, Renland, GISP2) over glacial-interglacial timescales based on the modern temperature-$\delta^{18}O_{precip}$ relation is problematic (Jouzel et al., 1997). The magnitude of deglacial warming in Greenland is known to be ~20 °C based on borehole thermometry (Cuffey et al., 1995; Johnsen et al., 1995). However, only half of this warming is accounted for if the modern local temperature-$\delta^{18}O_{precip}$ calibration is applied to the Greenland ice core $\delta^{18}O$ records (Johnsen et al., 2001). This apparent failure of the isotopic thermometer has been simulated by GCMs under full glacial boundary conditions, and reflects a major reduction of Greenland winter precipitation, and thus diminished representation of winter temperatures in the $\delta^{18}O$ record (Werner et al., 2000). Both Greenland and the Klondike serve as cautionary examples of the importance of considering precipitation seasonality when interpreting water isotopes in relict ice, and other water isotope proxies that integrate year-round precipitation such as hydrated volcanic glass shards and fossil plant waxes.

4.5. Hydrated volcanic glass shards

The Dawson tephra from Goldbottom Creek is hydrated to 2.3 wt % H_2O with a mean δD value of -241.5 ± 3‰ (Table 1). Using Equation (4), the δD of the secondary hydration waters is estimated to be -214.6 ± 3.3‰. This value is consistent with the Goldbottom pore ice δD mean of -218.7 ± 6.0‰, and suggests the secondary hydration waters are, within error, the same as those integrated by pore ice. A small offset between mean δD values, ~4‰ here, is not unexpected given that the initial magmatic water content of rhyolitic glass is variable (~0.1–0.3 wt%), with a δD range from −120‰ to −140‰ (Castro et al., 2014), and would tend to pull the bulk glass δD to slightly more enriched values assuming a higher initial water content. For most well-hydrated tephras (e.g., 3.5 wt%), the starting magmatic water typically accounts for less than 10% of total water and has a negligible effect on the δD_{precip} estimate (Friedman et al., 1993b). However, for less hydrated tephras such as the Dawson tephra (2.3 wt%), the δD_{precip} estimate could be influenced by magmatic water, and may require correction (Friedman et al., 1993b). Assuming initial water end members for rhyolites, 0.1 and 0.3 wt% (Friedman and Smith, 1958; Ross and Smith, 1955), and a δD of ~ −130‰ (Castro et al., 2014), we estimate a range of corrected δD_{precip} values from −218.4 to −227.3‰ (±3.3‰) for the Dawson tephra (see Supporting Information for calculations), which is again is consistent, within error, with the Goldbottom pore ice ($\delta D = -218.7 \pm 6.0$‰).

The relatively low hydration of the Dawson tephra (2.3%) implies incomplete hydration, since saturated rhyolitic tephras are capable of holding ~3.5 wt% water after a few millennia (Friedman et al., 1993b). Incomplete hydration might be considered unusual for most tephras that have been deposited for as long as the Dawson tephra (25.3 ^{14}C ka BP). However, the rapid burial history from loess deposition and concomitant permafrost aggradation would have limited the period of tephra-liquid interaction to roughly 400 years, assuming the same depositional model constraining the age of Quartz Creek pore ice (Supporting Information), after which the Dawson tephra would have sat below the permafrost table at negative ground temperatures. This limited period of tephra-liquid interaction may explain the relatively low hydration value observed for the Dawson tephra.

The presence of visible tephra bedded within ice-rich mucks offers a unique opportunity to compare δD_{precip} estimates from glass shards against known values from pore ice, and validate the empirical fractionation line of Friedman et al. (1993a) based their original study of post-depositional fluid inclusions in hydrated volcanic glass from Idaho. This line is routinely used in paleoaltimetry studies to estimate δD_{precip} from the δD of volcanic glass over Cenozoic time (e.g., Canavan et al., 2014; Fan et al., 2014). Our comparison of δD_{precip} estimates from the Dawson tephra and associated pore ice at Goldbottom confirms the Friedman et al. (1993a) line is robust, and demonstrates the potential to make robust estimates of δD_{precip} and climate from other Cenozoic tephras in Eastern Beringia where pore ice may by unavailable (Preece et al., 2011).

4.6. Fossil plant waxes

Pautler et al. (2014) calculated an average MAT depression of ~6 °C below modern for the MIS 4 and 3/2 time slices based on their *n*-C_{29} δD_{wax} data. Regionally averaged δD_{wax} values from the Pautler et al. (2014) dataset are -272.8 ± 6.4‰ (1σ, n = 9) and -268.5 ± 8.6‰ (1σ, n = 13) for MIS 4 and 3/2, respectively (Table 2; see Table 1 for δD_{wax} averaged by site). Based on these same data, we find that colder paleotemperature estimates are justified. Paleotemperatures based on these data are sensitive to several factors to varying degrees, which we explore below.

Knowledge of the modern δD_{precip} climatology is first needed as a baseline against which reconstructed δD_{precip} values can be compared. The difference between modern and reconstructed δD_{precip} can be equated to a temperature difference, given an appropriate transfer function (Eq. (5)). Pautler et al. (2014) estimated a modern δD_{precip} baseline based on measurements of δD_{wax} from a modern grassland soil near Kluane Lake, S.W. Yukon, and an $\varepsilon_{wax/precip}$ of −149‰ to complete the δD_{precip} estimate. We follow a different approach and define the modern δD_{precip} baseline directly from local knowledge of δD_{precip} based on relict ice and the Mayo GNIP record.

The paleotemperature estimates by Pautler et al. (2014) are influenced by the following three approximations: an 8‰ δD_{sw} correction; the Dansgaard (1964) temperature-δD_{precip} line; and an $\varepsilon_{wax/precip}$ of −149‰ ± 27‰. As discussed above, a δD_{sw} correction of 5‰ and Equation (5) are justified for the time slices of interest and region, with the latter having a larger influence on the result. However, the value of $\varepsilon_{wax/precip}$ needed to estimate δD_{precip} from δD_{wax} has the greatest impact on the final result.

Pautler et al. (2014) assumed the contributing paleoflora was predominantly C_3 grasses, as supported by a biomolecular compositional analysis of the muck deposits (Pautler et al., 2013). The $\varepsilon_{wax/precip}$ of −149‰ ± 27‰ (1σ, n = 49) is the mean $\varepsilon_{wax/precip}$ for C_3 graminoids based on a global $\varepsilon_{wax/precip}$ dataset, albeit one that is spatially biased towards low- and mid-latitude sites (Sachse et al., 2012). If this $\varepsilon_{wax/precip}$ value is used, the δD_{wax} averages for

MIS 4 and 3/2 (-272.8 ± 6.4‰ and -268.5 ± 8.6‰, respectively) could then be equated to annual δD_{precip} estimates of -151 ± 28‰ (1c.σ) and -145 ± 28‰ (1c.σ) respectively, after correcting for δD_{sw}. These δD_{precip} estimates are roughly equal to the isotopic composition of modern summer rains at Mayo (Jun-Jul mean = −149‰) and enriched by 25–31‰ compared to mean annual precipitation at Mayo (−176‰). Such δD_{precip} estimates are difficult to reconcile with expectations for a cold, glacial climate, and leads us to suspect that the fractionation based on temperate C_3 grasses is too large.

There are two compelling reasons to expect a smaller fractionation. The first is that the Klondike paleoflora was likely dominated by forbs and to a lesser extent by grasses, as recently revealed by sedimentary DNA (Willerslev et al., 2014) from the same Goldbottom and Quartz Creek sites of Pautler et al. (2014). Although the plant wax contributions of grasses and forbs may be compromised by taphonomic biases in the fossil record, it seems reasonable to adopt a fractionation that represents the apparently forb-dominated ecology. The $\varepsilon_{wax/precip}$ mean for forbs is less well constrained globally, but appears to be ~20‰ smaller than that of C_3 graminoids (Sachse et al., 2012). However, fractionations appropriate for these high latitudes may be even smaller than the global mean (Feakins et al., 2012; Shanahan et al., 2013; Wilkie et al., 2013; Yang et al., 2009; 2011). Smaller fractionations at high latitude sites have been linked to increased evapotranspiration caused by longer sunlight hours during Arctic summers (Yang et al., 2009) or alternatively could be linked to the greater use of stored carbohydrates (Sessions, 2006). A recent study of *n*-alkanoic acids in lake sediments from forb-shrub tundra catchments on Baffin Island, Canadian High Arctic, found a mean $\varepsilon_{wax/precip}$ of -61 ± 20‰ (Shanahan et al., 2013). A slightly larger $\varepsilon_{wax/precip}$ of -96 ± 8‰ was calculated from fossil plant waxes in recently deposited (*ca.* last 200 years) lake sediments in Lake El'gygytgyn, Eastern Siberia (Wilkie et al., 2013), a basin characterised today by open, low-lying vegetation types including grasses, forbs, bryophytes and sparse shrubs (Lozhkin et al., 2007; Wilkie et al., 2013).

The value of $\varepsilon_{wax/precip}$ cannot normally be determined for past ecosystems given that only the waxes remain in sediments in most contexts. However, in the permafrost of Eastern Beringia it is possible to directly determine the fractionation based on the offset between frozen water and sedimentary plant waxes from steppe-tundra plants. Using Equation (2), we calculate a $\varepsilon_{wax/precip}$ of -59 ± 10‰ (1c.σ) for the steppe-tundra based on the MIS 3/2 δD_{wax} average (-268.5 ± 8.6‰) and a δD_{precip} approximation based on mean Goldbottom and Quartz Creek pore ice (-222.3 ± 4.8‰). Here, we also newly report a δD_{wax} mean of -268.9 ± 2.7‰ (1σ, n = 7) based on alkanoic acids of the *n*-C_{28} chain-length (Supporting Information) from one of the Quartz Creek samples examined for pore ice, leading us to a similar $\varepsilon_{wax/precip}$ of -55 ± 3‰ (1c.σ), if the Quartz Creek pore ice δD mean is used as the δD_{precip} input. The $\varepsilon_{wax/precip}$ fractionations calculated here for *n*-alkanes and *n*-alkanoic acids from steppe-tundra plants are, within uncertainty, the same as high latitude estimates for modern plant *n*-alkanes (Yang et al., 2009; 2011) and *n*-alkanoic acids (Shanahan et al., 2013).

Our $\varepsilon_{wax/precip}$ estimate of -59 ± 10‰ for the Klondike steppe-tundra is small relative to the range of fractionations observed globally (Sachse et al., 2012), but consistent with recent evidence for smaller fractionations at higher latitudes. Based on this $\varepsilon_{wax/precip}$, we can estimate δD_{precip} and paleotemperatures for all Klondike muck deposits where *n*-C_{29} δD_{wax} values are available (Pautler et al., 2014). Based on the MIS 4 δD_{wax} average (-272.8 ± 6.4‰), we calculate that annual δD_{precip} during MIS 4 was depleted by ~56‰ relative to today after correcting for δD_{sw} by 5‰ (Table 2). We equate this offset to a maximum depression of MATs of ~18 ± 5 °C below modern (Table 3).

4.7. Other proxy-based reconstructions

Other estimates of Late Pleistocene paleotemperatures in Eastern Beringia have been based primarily upon fossil insects and pollen assemblages from lake sediments, mucks and paleosols. We briefly review some insights gained and limitation of these other proxy types for comparison with the water isotope proxies examined here. Fossil insect assemblages have yielded warm-season temperature (T_{max}) depressions for interior sites in Yukon and Alaska based on the MCR approach, with an overall T_{max} depression of ~4 ± 1 °C below modern during MIS 4 to 2 (Elias, 2001). The T_{min} variable was also estimated based on these same insect data, and indicates that T_{min} during MIS 4 to 2 was ~4 ± 4 °C warmer than today (Elias, 2001). However, insect-based T_{min} estimates should be interpreted with caution in northern regions. As discussed previously, insects are not skillful predictors of winter temperatures in northern regions (1σ = ±10 °C) since they are not exposed to winter air temperatures. They live underground or in leaf litter during winter where the microclimate remains close to the freezing point (Elias, 2001). A warmer-than-modern cold-season is unlikely for the Late Pleistocene, and is inconsistent with our water isotope data from ice wedges that indicate cold-season temperatures were ~14 ± 5 °C colder than today. Extreme winter cooling has also been inferred in northern Alaska for Younger Dryas time based a ~6‰ reduction in $\delta^{18}O$ recorded in the Barrow Ice Wedge System (Meyer et al., 2010), suggesting cold-season temperatures during periods of glacial advance were much colder, not warmer, than present.

Pollen records in Eastern Beringia have been used to estimate full glacial temperatures based on the modern analogue technique (Viau et al., 2008). In principle, the modern analogue technique evaluates fossil pollen spectra and finds the 'best' analogue(s) in a spatial network of modern pollen records for which present-day climates are known (e.g., North American Pollen Database). The distinction between an acceptable analogue and a non-analogue is a decision for the analyst, and is typically set by a quantitative dissimilarity threshold (Overpeck et al., 1985). The number of analogues retained and how local climates for each analogue are integrated into a paleoclimate estimate are also decisions for the analyst (Overpeck et al., 1985). Application of this method in Eastern Beringia, however, is complicated by the fact that there may be no true modern analogue for the steppe-tundra paleoflora, resembling both mid-latitude grasslands and forb-rich Arctic and Alpine tundra (Zazula et al., 2003; 2007). As a result, this method produces a range of disparate paleotemperatures, warmer-than-present to cooler-than-present depending on site (Bartlein et al., 2011). This disparity is related to the similarity of fossil pollen types to both mid-latitude grassland and Arctic tundra ecotypes (dissimilarity threshold is satisfied for both), which have no climatic overlap today.

In some cases, fossil pollen records have more in common with mid-latitude grasslands where the modern climate is warmer than present-day Eastern Beringia, while others have more in common with Arctic tundra where the modern climate is colder than present-day Eastern Beringia. Calculating the mean paleoclimate estimate from a bi-modal distribution of modern analogues from disparate latitudes and climates is susceptible to statistical error, or the 'wrong-analogue' problem described by Bartlein et al. (2011). A regional mean annual paleotemperature for Eastern Beringia was calculated by Viau et al. (2008) to be just ~3 °C colder than modern, reflecting a sub-Arctic comprise between mid-latitude and Arctic modern analogues. However, this estimate is significantly influenced by a decision to exclude two prairie-like pollen records, Tiinkdul and Rebel Lake (Viau et al., 2008). Viau et al. (2008) imply that including these sites in the regional estimate leads to an unreasonably warm paleoclimate, and excluding them results in a

'more reasonable' colder-than-modern full glacial.

The MAT depression of ~3 °C below modern (Viau et al., 2008) is anomalously warm in the broader Northern Hemisphere context of pollen-based paleotemperatures, which indicates depressions of ~8 °C below modern south of the Laurentide margin and a trend towards larger depressions at higher latitudes (Bartlein et al., 2011). A depression of ~3 °C is also insufficient to explain the large changes in relict ice isotopic composition we observe in the Klondike. While some of this discrepancy may be explained by uncertainties with the pore ice proxy, as discussed above, the potential wrong-analogue complications in using the modern analogue technique to interpret Eastern Beringian pollen is, we think, the more significant source of uncertainty.

All proxies have strengths and limitations. The insect MCR proxy is considered to be a good proxy for warm-season temperatures. Assuming the insects reliably constrain the warm-season temperature depression (~ 5–7 °C colder than modern for MIS 4 to 2, Klondike region; Zazula et al., 2007; 2011) and that the wedge ice isotopic composition reliably constrains the cold-season temperature depression (~14 °C below modern for MIS 3/2; this study), it may be reasonable to approximate the MAT depression using the median of the two seasonal estimates (~10 °C below modern), which takes advantage of the strengths of the different proxy types. However, improving the temporal resolution of this estimate is worth pursuing, but will require future sampling to augment the Klondike ice wedge dataset (currently n = 3).

Multi-proxy perspectives are needed to improve constraints on past climate in Eastern Beringia, expanding upon evidence from traditional proxies (e.g., fossil pollen and insects), as new proxies may corroborate, question or refine temperature estimates and lead to new insights. Pautler et al.'s (2014) recently added temperature estimates based on sedimentary δD_{wax} as well as temperature estimates from branched Glycerol Diakyl Glycerol Tetraethers (GDGTs) derived from fossil membrane lipids of soil bacteria represent progress towards increasing the diversity of multi-proxy reconstructions in this region. The degree of methylation (MBT) and cyclization (CBT) of branched GDGTs is sensitive to soil pH and mean temperature. Controlling for pH, the GDGT proxy has been calibrated with respect to annual temperature (Peterse et al., 2012). Mean paleotemperatures for the Klondike based on the GDGT proxy were found to be sensitive to how the MBT-CBT index is calculated (Pautler et al., 2014), either the original MBT-CBT calibration index of Weijers et al. (2007) or the modified MBT′-CBT calibration of Peterse et al. (2012). The Weijers et al. (2007) calibration reconstructs MATs for MIS 4 and 3/2 that are indifferent from modern, while the Peterse et al. (2012) calibration reconstructs MATs during these intervals that were 6 °C warmer than present.

A paleoclimate that is indifferent (or much warmer) compared to modern is again surprising for a high latitude region during glacial times, and raises doubts about whether the GDGT proxy is regionally appropriate. Calibration remains an ongoing effort in GDGT studies (De Jonge et al., 2014; Peterse et al., 2012; Weijers et al., 2007). We note that the calibration range of the GDGT proxy is largely restricted to temperate and tropical latitudes with MATs above 0 °C (Peterse et al., 2012). Furthermore, the linear response of the GDGT proxy appears to breakdown in arid regions where mean annual precipitation is less than 500 mm (Peterse et al., 2012). The modern climate of the Klondike region pushes the limits of the GDGT proxy in both regards (MAT ≈ −4 °C and MAP ≈ 325 mm at Dawson; Environment Canada). Considering that this region was probably significantly drier and colder during the last glacial on the basis of fossil evidence (Zazula et al., 2003), the current GDGT calibrations may not yet be well suited for reconstructing absolute Late Pleistocene temperatures in Eastern Beringia. Further development of the GDGT proxy in cold, dry Arctic regions is needed to resolve uncertainties in these reconstructions.

Fossil plant wax studies have considerable potential to augment the spatial resolution of paleoclimate fields across northern permafrost regions, as plant waxes are well preserved in organic rich soils in perennially frozen ground (this study), as well as lakes (Wilkie et al., 2013) and marine sediments (Pagani et al., 2006). This study provides proof of concept and opens the door for spatial studies of precipitation isotopes in permafrost plant wax deposits. Also, where visible tephra occur, additional δD_{precip} estimates can be made based on the hydration water δD, although volcanic deposits are spatially and temporally less extensive than plant waxes. Where they do occur, they also carry uniquely strong age dating potential making for very secure chronological contributions (Froese et al., 2008; 2009; Preece et al., 2011; Zazula et al., 2006).

We note there is also considerable potential to increase the number of paleotemperature estimates based on relict ice in northern regions (Meyer et al., 2015; Opel et al., 2011; Popp et al., 2006; Wetterich et al., 2014), as we demonstrated here. Motivation for expanding relict ice data collection would be to improve the spatial resolution of temperature estimates in the high latitude regions which are highly sensitive to climate change (Rohling et al., 2012), and across major climate transitions (Johnsen et al., 2001), not yet well resolved in the unglaciated northern regions. However, expanding the Klondike ice wedge dataset to cover Pleistocene stadials will take some time as ice wedges appear to be rare and thin, suggesting minimal development during full glacial times (Kotler and Burn, 2000), making this task analogous to looking for needles in a frozen haystack.

5. Conclusions

Water isotopes are powerful indicators of past climate change in high latitude regions, and mucks in Eastern Beringia are a rich archive for multiple water isotope proxies. Especially unique is the opportunity to constrain the net fractionations of proxies such as hydrated volcanic glass shards and fossil plant waxes by their direct comparison with paleoprecipitation in relict ice. This unique situation has allowed us to demonstrate a similar glass-water fractionation to that derived by Friedman et al. (1993a) for hydrated glass at warmer climate conditions, establishing that this process is not strongly temperature dependent, and for the first time empirically estimate the $\varepsilon_{wax/precip}$ of the Klondike steppe-tundra. We have drawn paleotemperature estimates for three Late Pleistocene time slices based on the available water isotope proxy data, and have defined temperature-precipitation isotope transfer functions that are calibrated for Eastern Beringia and northern North America. Our results indicate some of the largest paleotemperature depressions reconstructed in this region, and provide the first geochemical evidence for dry summers during Late Pleistocene cold stages. The putative precipitation seasonality change imparted a strong cold-season bias on the water isotope proxies that integrate year-round precipitation, including relict pore ice, volcanic glass shards and plant waxes. As such, estimates of the MAT depression based on these proxies are most appropriately interpreted as upper-bound limits. Improving estimates of the MAT depression based on these proxies may be possible, but would require re-calibrated transfer functions to account for precipitation seasonality through the glacial-interglacial transition. We posit that ice wedges provide a relatively consistent sample of cold-season precipitation, thus minimizing complications of a shifting precipitation seasonality, and allows for robust cold-season paleotemperature estimates. This multi-proxy effort highlights how insights from multiple archives of precipitation isotopes can clarify complications in fractionations (where appropriate), precipitation

seasonality and temperature conversions (in all proxies) towards more rigorous and nuanced insights into past precipitation and temperature changes. Each of the presented proxies offers great potential for more widespread applications in the unglaciated high latitudes where permafrost exists, to greatly improve upon our spatial reconstructions of temperature fields and thus our understanding of climate dynamics.

Acknowledgements

We thank the Klondike Placer Miners for access to the sites. We also thank Claude Hillaire-Marcel (Editor), Michael Hren and one anonymous reviewer for their constructive comments. This research was supported by an I.W. Killam Memorial Postdoctoral Fellowship to TJP, and an NSERC Discovery Grant and Northern Research Supplement to DGF.

Appendix A. Supplementary data

Supplementary data related to this article can be found at http://dx.doi.org/10.1016/j.quascirev.2016.02.006.

References

Aemisegger, F., Pfahl, S., Sodemann, H., Lehner, I., Seneviratne, S.I., Wernli, H., 2014. Deuterium excess as a proxy for continental moisture recycling and plant transpiration. Atmos. Chem. Phys. 14, 4029–4054.
Bartlein, P.J., Harrison, S.P., Brewer, S., Connor, S., Davis, B.A.S., Gajewski, K., et al., 2011. Pollen-based continental climate reconstructions at 6 and 21 ka: a global synthesis. Clim. Dyn. 37, 775–802.
Birks, S.J., Edwards, T.W.D., 2009. Atmospheric circulation controls on precipitation isotope-climate relations in western Canada. Tellus B 61, 566–576.
Braconnot, P., Harrison, S.P., Kageyama, M., Bartlein, P.J., Masson-Delmotte, V., Abe-Ouchi, A., et al., 2012. Evaluation of climate models using palaeoclimatic data. Nat. Clim. Change 2, 417–424.
Bryson, R.A., 1966. Air masses, streamlines, and the boreal forest. Geogr. Bull. 8, 228–269.
Calmels, F., Froese, D.G., Clavano, W.R., 2012. Cryostratigraphic record of permafrost degradation and recovery following historic (1898–1992) surface disturbances in the Klondike region, central Yukon Territory. Can. J. Earth Sci. 49, 938–952.
Canavan, R.R., Carrapa, B., Clementz, M.T., Quade, J., DeCelles, P.G., Schoenbohm, L.M., 2014. Early Cenozoic uplift of the Puna Plateau, Central Andes, based on stable isotope paleoaltimetry of hydrated volcanic glass. Geology 42, 447–450.
Castro, J.M., Bindeman, I.N., Tuffen, H., Ian Schipper, C., 2014. Explosive origin of silicic lava: textural and δD–H_2O evidence for pyroclastic degassing during rhyolite effusion. Earth Planet. Sci. Lett. 405, 52–61.
Craig, H., 1961. Isotopic variations in meteoric waters. Science 133, 1702–1703.
Cuffey, K.M., Clow, G.D., Alley, R.B., Stuiver, M., Waddington, E.D., Saltus, R.W., 1995. Large Arctic temperature change at the Wisconsin-Holocene glacial transition. Science 270, 455–458.
Dansgaard, W., 1964. Stable isotopes in precipitation. Tellus 16, 436–468.
De Jonge, C., Hopmans, E.C., Zell, C.I., Kim, J.-H., Schouten, S., Sinninghe Damsté, J.S., 2014. Occurrence and abundance of 6-methyl branched glycerol dialkyl glycerol tetraethers in soils: implications for palaeoclimate reconstruction. Geochimica Cosmochimica Acta 141, 97–112.
Edwards, T.W.D., Wolfe, B., Gibson, J.J., Hammarlund, D., 2004. Use of water isotope tracers in high-latitude hydrology and paleohydrology. In: Pienitz, R., Douglas MS, V., Smol, J.P. (Eds.), Long-term Environmental Change in Arctic and Antarctic Lakes. Kluwer Academic Publishers, Dordrecht, The Netherlands, pp. 187–207.
Edwards, T.W.D., Wolfe, B.B., MacDonald, G.M., 1996. Influence of changing atmospheric circulation on precipitation $\delta^{18}O$-temperature relations in Canada during the Holocene. Quat. Res. 46, 211–218.
Eglinton, G., Hamilton, R.J., 1967. Leaf epicuticular waxes. Science 156, 1322–1335.
Elias, S.A., 2001. Mutual climatic range reconstructions of seasonal temperatures based on late Pleistocene fossil beetle assemblages in Eastern Beringia. Quat. Sci. Rev. 20, 77–91.
Fan, M., Heller, P., Allen, S.D., Hough, B.G., 2014. Middle Cenozoic uplift and concomitant drying in the central Rocky Mountains and adjacent Great Plains. Geology 42, 547–550.
Feakins, S.J., Warny, S., Lee, J.-E., 2012. Hydrologic cycling over Antarctica during the middle Miocene warming. Nat. Geosci. 5, 557–560.
Fraser, T.A., Burn, C.R., 1997. On the nature and origin of "muck" deposits in the Klondike area, Yukon Territory. Can. J. Earth Sci. 34, 1333–1344.
French, H., Shur, Y., 2010. The principles of cryostratigraphy. Earth Sci. Rev. 101, 190–206.
Friedman, I., Gleason, J., Sheppard, R., Gude, A., 1993a. Deuterium fractionation as water diffuses into silicic volcanic ash. In: Swart, P., Lohmann, K., Mckenzie, J., Savin, S. (Eds.), Climate Change in Continental Isotopic Records. American Geophysical Union, Washington D.C, pp. 321–323.
Friedman, I., Gleason, J., Warden, A., 1993b. Ancient climate from deuterium content of water in volcanic glass. In: Swart, P., Lohmann, K., Mckenzie, J., Savin, S. (Eds.), Climate Change in Continental Isotopic Records. American Geophysical Union, Washington D.C, pp. 309–319.
Friedman, I., Smith, R.L., 1958. The deuterium content of water in some volcanic glasses. Geochimica Cosmochimica Acta 15, 218–228.
Fritz, M., Wetterich, S., Schirrmeister, L., Meyer, H., Lantuit, H., Preusser, F., et al., 2012. Eastern Beringia and beyond: late Wisconsinan and Holocene landscape dynamics along the Yukon Coastal Plain, Canada. Palaeogeogr. Palaeoclimatol. Palaeoecol. 319–320, 28–45.
Froese, D.G., Westgate, J.A., Reyes, A.V., Enkin, R.J., Preece, S.J., 2008. Ancient permafrost and a future, warmer Arctic. Science 321, 1648.
Froese, D.G., Zazula, G.D., Reyes, A.V., 2006. Seasonality of the late Pleistocene Dawson tephra and exceptional preservation of a buried riparian surface in central Yukon Territory, Canada. Quat. Sci. Rev. 25, 1542–1551.
Froese, D.G., Zazula, G.D., Westgate, J.A., Preece, S.J., Sanborn, P.T., Reyes, A.V., et al., 2009. The Klondike goldfields and Pleistocene environments of Beringia. GSA Today 19, 4–10.
Gat, J.R., Bowser, C., Kendall, C., 1994. The contribution of evaporation from the Great Lakes to the continental atmosphere; estimate based on stable isotope data. Geophys. Res. Lett. 21, 557–560.
Gat, J.R., Klein, B., Kushnir, Y., Roether, W., Wernli, H., Yam, R., et al., 2003. Isotope composition of air moisture over the Mediterranean Sea: an index of the air–sea interaction pattern. Tellus B 55, 953–965.
IAEA/WMO, 2014. Global Network of Isotopes in Precipitation. The GNIP Database. Available at: http://www.iaea.org/water.
Johnsen, S.J., Dahl-Jensen, D., Dansgard, W., Gundestrup, N., 1995. Greenland palaeotemperatures derived from GRIP bore hole temperature and ice core isotope profiles. Tellus B 47, 624–629.
Johnsen, S.J., Dahl-Jensen, D., Gundestrup, N., Steffensen, J.P., Clausen, H.B., Miller, H., et al., 2001. Oxygen isotope and palaeotemperature records from six Greenland ice-core stations: Camp Century, Dye-3, GRIP, GISP2, Renland and NorthGRIP. J. Quat. Sci. 16, 299–307.
Jouzel, J., 2013. A brief history of ice core science over the last 50 yr. Clim. Past Past 9, 2525–2547.
Jouzel, J., Alley, R.B., Cuffey, K.M., Dansgaard, W., Grootes, P., Hoffmann, G., et al., 1997. Validity of the temperature reconstruction from water isotopes in ice cores. J. Geophys. Res. 102, 471–487.
Jouzel, J., Merlivat, L., 1984. Deuterium and oxygen 18 in precipitation: modeling of the isotopic effects during snow formation. J. Geophys. Res. 89, 11749–11757.
Jouzel, J., Stiévenard, M., Johnsen, S.J., Landais, A., Masson-Delmotte, V., Sveinbjörnsdottir, A., et al., 2007. The GRIP deuterium-excess record. Quat. Sci. Rev. 26, 1–17.
Jouzel, J., Vimeux, F., Caillon, N., Delaygue, G., Hoffmann, G., Masson-Delmotte, V., et al., 2003. Magnitude of isotope/temperature scaling for interpretation of central Antarctic ice cores. J. Geophys. Res. 108 http://dx.doi.org/10.1029/2002JD002677.
Kalnay, E., Kanamitsu, M., Kistler, R., Collins, W., Deaven, D., Gandin, L., et al., 1996. The NCEP/NCAR 40-year reanalysis project. Bull. Am. Meteorological Soc. 77, 437–471.
Kotler, E., Burn, C.R., 2000. Cryostratigraphy of the Klondike "muck" deposits, west-central Yukon Territory. Can. J. Earth Sci. 37, 849–861.
Lacelle, D., Lauriol, B., Clark, I.D., Cardyn, R., Zdanowicz, C., 2007. Nature and origin of a Pleistocene-age massive ground-ice body exposed in the Chapman Lake moraine complex, central Yukon Territory, Canada. Quat. Res. 68, 249–260.
Lachenbruch, A.H., 1962. Mechanics of thermal contraction cracks and ice-wedge polygons in permafrost. Geol. Soc. Am. Special Pap. 70, 1–66.
Lackman, G.M., Gyakum, J.R., 1996. The synoptic- and planetary-scale signatures of precipitating systems over the Mackenzie River Basin. Atmos. Ocean 34 (4), 647–674.
LeGrande, A.N., Schmidt, G.A., 2009. Sources of Holocene variability of oxygen isotopes in paleoclimate archives. Clim. Past 5, 441–455.
Lisiecki, L.E., Raymo, M.E., 2005. A Pliocene-Pleistocene stack of 57 globally distributed benthic $\delta^{18}O$ records. Paleoceanography 20. http://dx.doi.org/10.1029/2004PA001071.
Lozhkin, A.V., Anderson, P.M., Matrosova, T.V., Minyuk, P.S., 2007. The pollen record from El'gygytgyn Lake: implications for vegetation and climate histories of northern Chukotka since the late middle Pleistocene. J. Paleolimnol. 37, 135–153.
Mackay, J.R., 1983. Downward water movement into frozen ground, western arctic coast, Canada. Can. J. Earth Sci. 20, 120–134.
Mackay, J.R., 1993. Air temperature, snow cover, creep of frozen ground, and the time of ice-wedge cracking, western Arctic coast. Can. J. Earth Sci. 30, 1720–1729.
Malone, M.J., Martin, J.B., Schönfeld, J., Ninnemann, U.S., Nürnburg, D., White, T.S., 2004. The oxygen isotopic composition and temperature of Southern Ocean bottom waters during the last glacial maximum. Earth Planet. Sci. Lett. 222, 275–283.
Merlivat, L., Jouzel, J., 1979. Global climatic interpretation of the deuterium-oxygen 18 relationship for precipitation. J. Geophys. Res. 84, 5029–5033.
Meyer, H., Opel, T., Laepple, T., Dereviagin, A.Y., Hoffmann, K., Werner, M., 2015.

Long-term winter warming trend in the Siberian Arctic during the mid- to late Holocene. Nat. Geosci. 8, 122–125.
Meyer, H., Schirrmeister, L., Yoshikawa, K., Opel, T., Wetterich, S., Hubberten, H.-W., et al., 2010. Permafrost evidence for severe winter cooling during the Younger Dryas in northern Alaska. Geophys. Res. Lett. 37 http://dx.doi.org/10.1029/2009GL041013.
Nolan, G., Bindeman, I.N., 2013. Experimental investigation of rates and mechanisms of isotope exchange (O, H) between volcanic ash and isotopically-labeled water. Geochimica Cosmochimica Acta 111, 5–27.
Opel, T., Dereviagin, A.Y., Meyer, H., Schirrmeister, L., Wetterich, S., 2011. Palaeoclimatic information from stable water isotopes of Holocene ice wedges on the Dmitrii Laptev Strait, northeast Siberia, Russia. Permafr. Periglac. Process. 22, 84–100.
Overpeck, J.T., Webb III, T., Prentice, I., 1985. Quantitative interpretation of fossil pollen spectra: dissimilarity coefficients and the method of modern analogs. Quat. Res. 23, 87–108.
Pagani, M., Pedentchouk, N., Huber, M., Sluijs, A., Schouten, S., Brinkhuis, H., et al., 2006. Arctic hydrology during global warming at the Palaeocene/Eocene thermal maximum. Nature 442, 671–675.
Pautler, B.G., Reichart, G.-J., Sanborn, P.T., Simpson, M.J., Weijers, J.W.H., 2014. Comparison of soil derived tetraether membrane lipid distributions and plant-wax δD compositions for reconstruction of Canadian Arctic temperatures. Palaeogeogr. Palaeoclimatol. Palaeoecol. 404, 78–88.
Pautler, B.G., Sanborn, P.T., Simpson, A.J., Simpson, M.J., 2013. Molecular characterization of organic matter in Canadian Arctic paleosols for paleoecological applications. Org. Geochem. 122–138.
Peterse, F., van der Meer, J., Schouten, S., Weijers, J.W.H., Fierer, N., Jackson, R.B., et al., 2012. Revised calibration of the MBT–CBT paleotemperature proxy based on branched tetraether membrane lipids in surface soils. Geochimica Cosmochimica Acta 96, 215–229.
Petrone, R.M., Rouse, W.R., 2000. Synoptic controls on the surface energy and water budgets in sub-arctic regions of Canada. Int. J. Climatol. 20, 1149–1165.
Pfahl, S., Sodemann, H., 2014. What controls deuterium excess in global precipitation? Clim. Past 10, 771–781.
Popp, S., Diekmann, B., Meyer, H., Siegert, C., Syromyatnikov, I., Hubberten, H.-W., 2006. Palaeoclimate signals as inferred from stable-isotope composition of ground ice in the Verkhoyansk foreland, Central Yakutia. Permafr. Periglac. Process. 17, 119–132.
Preece, S.J., Westgate, J.A., Froese, D.G., Pearce, N.J.G., Perkins, W.T., 2011. A catalogue of late Cenozoic tephra beds in the Klondike goldfields and adjacent areas, Yukon Territory. Can. J. Earth Sci. 48, 1386–1418.
Rohling, E.J., Foster, G.L., Grant, K.M., Marino, G., Roberts, A.P., Tamisiea, M.E., et al., 2014. Sea-level and deep-sea-temperature variability over the past 5.3 million years. Nature 508, 477–482.
Rohling, E.J., Medina-Elizalde, M., Shepherd, J.G., Siddall, M., Stanford, J.D., 2012. Sea surface and high-latitude temperature sensitivity to radiative forcing of climate over several glacial cycles. J. Clim. 25, 1635–1656.
Ross, C.S., Smith, R.L., 1955. Water and other volatiles in volcanic glasses. Am. Mineral. 40, 1071–1089.
Rozanski, K., Araguas-Araguas, L., Gonfiantini, R., 1993. Isotopic patterns in modern global precipitation. In: Swart, P.K., McKenzie, J., Lohmann, K.C., Savin, S. (Eds.), Climate Change in Continental Isotopic Records. American Geophysical Union, Washington D.C, pp. 1–37.
Sachse, D., Billault, I., Bowen, G.J., Chikaraishi, Y., Dawson, T.E., Feakins, S.J., et al., 2012. Molecular paleohydrology: interpreting the hydrogen-isotopic composition of lipid biomarkers from photosynthesizing organisms. Annu. Rev. Earth Planet. Sci. 40, 221–249.
Schirrmeister, L., Froese, D., Tumskoy, V., Grosse, G., Wetterich, S., 2013. Yedoma: Late Pleistocene ice-rich syngenetic permafrost of Beringia. In: Elias, S.A. (Ed.), The Encyclopedia of Quaternary Science. Elsevier, Amsterdam, pp. 542–552.
Schrag, D.P., Adkins, J.F., McIntyre, K., Alexander, J.L., Hodell, D.A., Charles, C.D., et al., 2002. The oxygen isotopic composition of seawater during the last glacial maximum. Quat. Sci. Rev. 21, 331–342.
Schwamborn, G., Meyer, H., Fedorov, G., Schirrmeister, L., Hubberten, H.-W., 2006. Ground ice and slope sediments archiving late Quaternary paleoenvironment and paleoclimate signals at the margins of El'gygytgyn impact Crater, NE Siberia. Quat. Res. 66, 259–272.
Sessions, A.L., 2006. Seasonal changes in D/H fractionation accompanying lipid biosynthesis in *Spartina alterniflora*. Geochimica Cosmochimica Acta 70, 2153–2162.
Shanahan, T.M., Hughen, K.A., Ampel, L., Sauer, P.E., Fornace, K., 2013. Environmental controls on the $^{2}H/^{1}H$ values of terrestrial leaf waxes in the eastern Canadian Arctic. Geochimica Cosmochimica Acta 119, 286–301.
Szeto, K.K., Stewart, R.E., Yau, M.K., Gyakum, J., 2008. The Mackenzie climate system: a synthesis of MAGS atmospheric research. In: Woo, M. (Ed.), Cold Region Atmospheric and Hydrologic Studies: the Mackenzie GEWEX Experience. Volume 1: Atmospheric Dynamics. Springer, New York, pp. 23–50.
Tierney, J.E., Russell, J.M., Huang, Y., Damsté, J.S.S., Hopmans, E.C., Cohen, A.S., 2008. Northern hemisphere controls on tropical southeast African climate during the past 60,000 years. Science 322, 252–255.
Viau, A.E., Gajewski, K., Sawada, M.C., Bunbury, J., 2008. Low- and high-frequency climate variability in eastern Beringia during the past 25000 years. Can. J. Earth Sci. 45, 1435–1453.
Weijers, J.W.H., Schouten, S., van den Donker, J.C., Hopmans, E.C., Sinninghe Damsté, J.S., 2007. Environmental controls on bacterial tetraether membrane lipid distribution in soils. Geochimica Cosmochimica Acta 71, 703–713.
Wendland, W.M., Bryson, R.A., 1981. Northern Hemisphere airstream regions. Mon. Weather Rev. 109, 255–270.
Werner, M., Heimann, M., 2002. Modelling interannual variability of water isotopes in Greenland and Antarctica. J. Geophys. Res. 107 http://dx.doi.org/10.1029/2001JD900253.
Werner, M., Mikolajewicz, U., Heimann, M., Hoffmann, G., 2000. Borehole versus isotope temperatures on Greenland: seasonality does matter. Geophys. Res. Lett. 27, 723–726.
Wetterich, S., Rudaya, N., Tumskoy, V., Andreev, A.A., Opel, T., Schirrmeister, L., et al., 2011. Last glacial maximum records in permafrost of the East Siberian Arctic. Quat. Sci. Rev. 30, 3139–3151.
Wetterich, S., Tumskoy, V., Rudaya, N., Andreev, A.A., Opel, T., Meyer, H., et al., 2014. Ice complex formation in arctic East Siberia during the MIS3 interstadial. Quat. Sci. Rev. 84, 39–55.
Wilkie, K.M.K., Chapligin, B., Meyer, H., Burns, S., Petsch, S., Brigham-Grette, J., 2013. Modern isotope hydrology and controls on δD of plant leaf waxes at Lake El'gygytgyn, NE Russia. Clim. Past 9, 335–352.
Willerslev, E., Davison, J., Moora, M., Zobel, M., Coissac, E., Edwards, M.E., et al., 2014. Fifty thousand years of Arctic vegetation and megafaunal diet. Nature 506, 47–51.
Yang, H., Liu, W., Leng, Q., Hren, M.T., Pagani, M., 2011. Variation in n-alkane δD values from terrestrial plants at high latitude: implications for paleoclimate reconstruction. Org. Geochem. 42, 283–288.
Yang, H., Pagani, M., Briggs, D.E.G., Equiza, M.A., Jagels, R., Leng, Q., et al., 2009. Carbon and hydrogen isotope fractionation under continuous light: implications for paleoenvironmental interpretations of the high Arctic during Paleogene warming. Oecologia 160, 461–470.
Zazula, G.D., Froese, D.G., Elias, S.A., Kuzmina, S., La Farge, C., Reyes, A.V., et al., 2006. Vegetation buried under Dawson tephra (25,300 ^{14}C years BP) and locally diverse late Pleistocene paleoenvironments of Goldbottom Creek, Yukon, Canada. Palaeogeogr. Palaeoclimatol. Palaeoecol. 242, 253–286.
Zazula, G.D., Froese, D.G., Elias, S.A., Kuzmina, S., Mathewes, R.W., 2007. Arctic ground squirrels of the mammoth-steppe: paleoecology of Late Pleistocene middens (~24000–29450 ^{14}C yr BP), Yukon Territory, Canada. Quat. Sci. Rev. 26, 979–1003.
Zazula, G.D., Froese, D.G., Elias, S.A., Kuzmina, S., Mathewes, R.W., 2011. Early Wisconsinan (MIS 4) Arctic ground squirrel middens and a squirrel-eye-view of the mammoth-steppe. Quat. Sci. Rev. 30, 2220–2237.
Zazula, G.D., Froese, D.G., Schweger, C.E., Mathewes, R.W., Beaudoin, A.B., Telka, A.M., et al., 2003. Palaeobotany: ice-age steppe vegetation in East Beringia. Nature 423, 603.